Research Square

Preprints are preliminary reports that have not undergone peer review.
They should not be considered conclusive, used to inform clinical practice,
or referenced by the media as validated information.

SLC2A1 promotes chemo-immunotherapy resistance in lung adenocarcinoma by modulating the AKT signaling pathway

Jingsheng Ruan
Jinshan Hospital of Fudan University
Mengxing Zhao
Jinshan Hospital of Fudan University
Ying Yuan
Jinshan Hospital of Fudan University
Jinlong Zhong
zhongjinlong2007@163.com

Jinshan Hospital of Fudan University

Research Article

Keywords: Lung adenocarcinoma, SLC2A1, AKT signaling pathway, Chemo-immunotherapy resistance

Posted Date: March 30th, 2026

DOI: https://doi.org/10.21203/rs.3.rs-8886496/v1

License: This work is licensed under a Creative Commons Attribution 4.0 International License.
Read Full License

Additional Declarations: No competing interests reported.

Version of Record: A version of this preprint was published at Functional & Integrative Genomics on October 28th, 2026. See the published version at https://doi.org/10.1007/s10142-026-02085-7.

SLC2A1 promotes chemo-immunotherapy resistance in lung adenocarcinoma by modulating the AKT signaling pathway

Jingsheng Ruan*, Mengxing Zhao*, Ying Yuan, Jinlong Zhong

Affiliation:
Department of Thoracic Surgery, Jinshan Hospital of Fudan University, Fudan University, Shanghai, China.

* These authors contributed equally to this work

Corresponding authors:

Ying Yuan
Department of Thoracic Surgery, Jinshan Hospital of Fudan University, Fudan University, No.1508 Longhang Road, Shanghai, 200540, China.
18930819857@163.com

Jinlong Zhong
Department of Thoracic Surgery, Jinshan Hospital of Fudan University, Fudan University, No.1508 Longhang Road, Shanghai, 200540, China.
zhongjinlong2007@163.com

Statements and Declarations

Competing interests

The authors declare no competing interests.

Abstract

Chemo-immunotherapy has become a standard treatment for lung adenocarcinoma (LUAD), yet the development of dual resistance to platinum-based chemotherapy and PD-1/PD-L1 blockade severely limits durable clinical benefit. This study aimed to identify a unified molecular regulator that concurrently drives chemoresistance and immune evasion. scRNA-seq of LUAD clinical cohorts was performed to characterize resistance-associated malignant subpopulations, followed by integrative bioinformatics analyses to screen key drivers. Clinical specimen validation and functional experiments, including CCK-8 assays, flow cytometry, transwell migration and western blotting, were conducted to elucidate the underlying mechanisms. We identified a malignant subcluster enriched in non-responsive patients and determined SLC2A1 as the unique overlapping candidate linked to therapeutic failure. Elevated SLC2A1 expression correlated with poor prognosis and enhanced AKT phosphorylation levels. Functionally, SLC2A1 promoted cisplatin resistance, suppressed apoptosis, increased migratory capacity, and upregulated PD-L1 expression, all of which were substantially reversed by AKT inhibition. Notably, this study suggests a previously underappreciated non-canonical role of SLC2A1 as an upstream modulator that coordinates the AKT-PD-L1 axis, thereby potentially integrating chemotherapy resistance and immune escape into a single regulatory framework. These findings provide mechanistic insight into dual refractory LUAD and establish the SLC2A1/AKT axis as a promising therapeutic vulnerability for precision intervention.

Keywords: Lung adenocarcinoma; SLC2A1; AKT signaling pathway; Chemo-immunotherapy resistance

Introduction

Lung adenocarcinoma (LUAD) remains the most prevalent histological subtype of lung cancer, representing a major contributor to global cancer-related mortality and showing a rising incidence worldwide (Siegel et al., 2021). Despite the clinical paradigm shift toward combination therapy with platinum-based chemotherapy and programmed cell death protein 1 inhibitors, the emergence of acquired therapeutic resistance remains a formidable barrier to long-term survival (Huang et al., 2025; Lahiri et al., 2023; Meyer et al., 2024). Treatment failure also imposes substantial socio-economic burdens, necessitating costly second-line interventions (Kessler et al., 2023). Although various genomic alterations and PD-L1 expression have been proposed as predictive markers, these factors alone do not fully explain the complex intracellular signaling networks underlying resistance to both cytotoxic chemotherapy and immune-mediated surveillance (Memon et al., 2024; Wang et al., 2025).

Currently, strategies to overcome LUAD resistance focus on targeting bypass signaling pathways or modulating the tumor microenvironment (TME) (Wang et al., 2025; Xu et al., 2025). However, a critical limitation persists: most current approaches treat chemotherapy resistance and immunotherapy evasion as independent phenomena, overlooking the possibility of a shared upstream regulator that simultaneously drives both processes through coordinated signal transduction (Tufail et al., 2025; Wang et al., 2025). Despite the extensive characterization of the AKT axis as a central mediator of cell survival, anti-apoptosis, and immune escape(Gao et al., 2023; Watterson and Coelho, 2023), the upstream mechanisms responsible for its sustained activation under chemo-immunotherapy pressure remain poorly defined. This knowledge gap underscores the need to identify novel signaling scaffolds that regulators dual resistance, as the lack of mechanistic clarity prevents the development of effective sensitizing agents to overcome therapeutic refractory states (Li et al., 2025; Yang et al., 2024) .

In the present study, we systematically investigated the non-canonical signaling role of Solute carrier family 2 member 1 (SLC2A1) in modulating the sensitivity of LUAD to chemo-immunotherapy. By integrating scRNA-seq analysis of clinical

cohorts with experimental validation, we identified SLC2A1 as a key driver of chemo-immunotherapy resistance, with overexpression significantly associated with unfavorable clinical outcomes. Mechanistically, we demonstrated that SLC2A1 serves as a critical upstream modulator that sustains AKT pathway activation, thereby bypassing cisplatin-induced pro-apoptotic signals and facilitating immune evasion. Furthermore, functional assays and rescue experiments demonstrated that genetic silencing or pharmacological inhibition of the SLC2A1/AKT axis suppresses proliferative capacity and mitigates the immunosuppressive phenotype of LUAD cells. Collectively, our findings elucidate a novel SLC2A1-AKT signaling mechanism underlying multi-modal treatment resistance and identify a potential therapeutic target for improving outcomes in refractory LUAD.

Materials and Methods

Clinical Specimen Collection and Processing

The study protocol was strictly designed and executed in compliance with the ethical guidelines of the Declaration of Helsinki and was formally approved by the Ethics Committee of Jinshan Hospital of Fudan University (Approval No. JIEC 2025-S32). Between January 2024 and January 2025, a total of 10 patients diagnosed with primary LUAD were recruited for this study. All participants were clinical candidates for platinum-based chemo-immunotherapy. Inclusion criteria were: (1) histologically confirmed LUAD; (2) no prior systemic anticancer therapy; (3) available surgical specimens. Following the initiation of therapy, clinical responses were rigorously monitored and evaluated by radiographic imaging every 6-9 weeks according to the Response Evaluation Criteria in Solid Tumors (RECIST v1.1). Patients were stratified into two cohorts: the Responder group (Complete Response, CR; Partial Response, PR) and the Non-responder group (Stable Disease, SD; Progressive Disease, PD). During surgical resection, tumor tissues and matched adjacent normal tissues were collected. To preserve the integrity of labile signaling molecules such as p-AKT and mRNA,

specimens were snap-frozen in liquid nitrogen within a strict 30-minute window post-resection and stored at -80°C until use. Histopathological verification was performed via Hematoxylin and Eosin staining by two senior board-certified pathologists to ensure a tumor purity of at least 70% for molecular analysis.

Bioinformatics Analysis of scRNA-seq Data

To dissect the molecular landscape of chemo-immunotherapy resistance, we utilized a multi-omics approach. scRNA-seq data from LUAD patient cohorts (GSE123902 (Laughney et al., 2020), Zenodo (accessible at https://zenodo.org/records/8227624) (Yan et al., 2025)) were processed using the Seurat R package (v4.0). The initial quality control pipeline was rigorous: cells were filtered to exclude those with fewer than 200 or more than 5000 unique feature counts, and cells with mitochondrial gene content exceeding 20% were discarded to eliminate dying or low-quality cells. Data were then normalized using the LogNormalize method with a scale factor of 10,000, and the top 2,000 highly variable genes were identified using the vst method Dimensionality reduction was performed by Principal Component Analysis (PCA) on the scaled data, followed by non-linear reduction using Uniform Manifold Approximation and Projection (UMAP). Cell clustering was executed using the FindNeighbors and FindClusters functions with a resolution parameter of 0.5. To pinpoint the malignant cells within the heterogeneous tumor microenvironment, we employed the inferCNV R package. Immune cells (T cells and B cells) within the same dataset were used as a diploid reference. A sliding window of 100 genes was applied across chromosomes to calculate the relative expression magnitude, confirming the malignant cells based on their high levels of chromosomal copy number variations. Subsequently, for functional annotation, Gene Set Enrichment Analysis (GSEA) was performed.

Cell Culture

Human LUAD cell lines, A549 and H1299, were purchased from the American Type Culture Collection (ATCC, Manassas, VA, USA). Both cell lines were maintained

in RPMI-1640 medium (Gibco, Waltham, MA, USA) supplemented with 10% heat-inactivated fetal bovine serum, 100 U/mL penicillin, and 100 μg/mL streptomycin. Cells were cultured in a humidified atmosphere containing 5% CO_2 at 37°C. All cell lines were authenticated via Short Tandem Repeat (STR) profiling and tested negative for Mycoplasma contamination using the MycoAlert detection kit (Lonza, Switzerland).

siRNA Transfection and Gene Modulation

Small interfering RNAs (siRNAs) targeting human SLC2A1 (si*SLC2A1*-1 and si*SLC2A1*-2) and a negative control siRNA (NC) were synthesized by GenePharma (Shanghai, China). The sequences were as follows: si*SLC2A1*-1, Forward: GCCUGUGUAUGCCACCAUUTT; Reverse: AAUGGUGGCAUACACAGGCTT; siSLC2A1-2, Forward: GCAUCAACGCUGUCUUCUATT; Reverse UAGAAGACAGCGUUGAUGCTT. Cells were seeded in six-well plates and transfected at 60-70% confluence using Lipofectamine 3000 (Invitrogen, Carlsbad, CA, USA) according to the manufacturer's instructions. Briefly, siRNAs were diluted in Opti-MEM, mixed with Lipofectamine 3000 reagent, and incubated for 15 minutes at room temperature before being added to the cells. After 48 hours of transfection, cells were harvested for subsequent experiments. The knockdown efficiency of SLC2A1 was confirmed at the protein level by western blotting.

Immunohistochemistry Staining

Formalin-fixed paraffin-embedded (FFPE) LUAD tissues were sectioned at 4 μm. The slides were baked at 65°C for 2 hours, deparaffinized in xylene three times (10 minutes each), and rehydrated through a graded series of ethanol (100%, 95%, 85%, and 75%). Antigen retrieval was conducted by immersing slides in 0.01 M sodium citrate buffer (pH 6.0) and heating in a microwave at high power for 5 minutes, followed by medium-low power for 15 minutes. To block endogenous peroxidase, sections were incubated in 3% hydrogen peroxide for 15 minutes in the dark. After blocking with 5% normal goat serum for 1 hour at room temperature, sections were incubated overnight at 4°C with primary antibodies: anti-SLC2A1 (Abcam, 1:200). Following three washes

with PBST, slides were incubated with HRP-conjugated secondary antibodies for 1 hour. The signal was visualized using a DAB substrate kit (Vector Laboratories, Burlingame, CA, USA) and counterstained with Mayer's hematoxylin.

CCK-8 Assay

Cell viability and drug sensitivity were quantified using the Cell Counting Kit-8 (CCK-8) (Dojindo, Kumamoto, Japan). Cells were harvested during the logarithmic growth phase and seeded into 96-well plates at a density of $2x10^3$ cells per well in 100 μL of medium. After 24 hours of attachment, the medium was replaced with 100 μL of fresh medium containing gradient concentrations of cisplatin (0, 5, 10, 20, 40, and 80 μM). Following a 48-hour incubation, 10 μL of CCK-8 reagent was added to each well, avoiding the formation of bubbles. The plates were incubated for an additional 2 hours at 37°C. The OD was measured at 450 nm using a microplate reader (Bio-Rad, Hercules, CA, USA). Each concentration was tested in three replicate wells. Cell viability was calculated using the following formula: Cell viability (%) = [(A_treated − A_blank) / (A_control − A_blank)] × 100%, where A_treated represents the absorbance of treated cells, A_control represents the absorbance of untreated control cells, and A_blank represents the absorbance of wells containing medium and CCK-8 reagent without cells. The half-maximal inhibitory concentration (IC_{50}) values were determined using GraphPad Prism 9.0 (GraphPad Software, San Diego, CA, USA) by nonlinear regression analysis with a log(inhibitor) versus normalized response-variable slope (four-parameter) model.

Wound Healing Assay

To assess the impact of the SLC2A1/AKT axis on horizontal cell migration, a wound healing assay was conducted. Cells were seeded in 6-well plates and grown to 100% confluence. A sterile 200 μL plastic pipette tip was used to create a linear wound by scratching the cell monolayer across the center of the well. The cells were washed three times with PBS to remove non-adherent cells and debris.

The culture medium was then replaced with serum-free RPMI-1640 to suppress cell proliferation, ensuring that the scratch closure was solely due to cell migration. Images were captured at 0 hours and 24 hours after wounding using an inverted microscope. The wound area was measured using ImageJ software (v1.53).

Flow Cytometry

Flow cytometry protocol was designed to analyze the immune and survival phenotypes of the cells. After 48 hours of cisplatin treatment with or without MK-2206 (a highly selective AKT inhibitor; Selleck Chemicals, Houston, TX, USA), cells (including those floating in the supernatant) were harvested and centrifuged at 1000 rpm for 5 minutes. The pellet was washed twice with ice-cold PBS. For PD-L1 surface staining, $1x10^6$ cells were resuspended in 100 µL of PBS and incubated with 5 µL of PE-conjugated anti-human PD-L1 antibody (BioLegend, San Diego, CA, USA) for 30 minutes at 4°C in the dark. After washing with PBS, cells were resuspended in 100 µL of 1X Binding Buffer. Subsequently, 5 µL of Annexin V-FITC and 5 µL of Propidium Iodide (PI) (BioLegend, San Diego, CA, USA) were added. The cells were incubated for 15 minutes at room temperature in the dark. Data acquisition was performed on a FACSCanto II flow cytometer (BD Biosciences). A minimum of 20,000 events were recorded per sample. Compensation beads were used to correct for spectral overlap between FITC, PE, and PI. Data were analyzed using FlowJo v10 software. Apoptosis was quantified as the percentage of Annexin V-positive cells, while PD-L1 expression was reported as the Mean Fluorescence Intensity (MFI) of the PE channel within the live cell population.

Western Blotting

Total protein was extracted from cells using RIPA Lysis Buffer supplemented with 1% Protease Inhibitor Cocktail and 1% Phosphatase Inhibitor Cocktail. Cells were lysed on ice for 30 minutes, followed by centrifugation at 12,000 rpm for 15 minutes at 4°C. Protein concentration was determined using the BCA Protein Assay Kit. Approximately 30 µg of protein per sample was denatured at 95°C for 5 minutes in

SDS loading buffer. The samples were separated by 10% SDS-PAGE and transferred onto 0.22-μm PVDF membranes (Millipore, Billerica, MA, USA). Membranes were blocked with 5% non-fat milk in TBST for 1 hour at room temperature. Primary antibodies against SLC2A1 (1:1000), p-AKT (Ser473) (1:1000), total AKT (1:1000), PD-L1 (1:1000), and GAPDH (1:5000) were incubated with the membranes overnight at 4°C. After three 10-minute washes with TBST, the membranes were incubated with HRP-conjugated secondary antibodies (1:5000) for 1 hour. Protein bands were visualized using an Enhanced Chemiluminescence (ECL) kit (Thermo Fisher) and captured using a ChemiDoc imaging system (Bio-Rad). Densitometric analysis was performed using ImageJ. For rescue experiments, ov*SLC2A1* cells were pre-treated with 2 μM MK-2206 for 24 hours prior to protein extraction or functional assays.

Statistical Analysis

All experiments were performed in at least three independent biological replicates. Data are presented as the mean ± standard deviation (SD). Statistical significance was determined using GraphPad Prism 9.0. For comparisons between two groups, a two-tailed Student's t-test was used. For multiple group comparisons, one-way analysis of variance (ANOVA) followed by Tukey's post-hoc test was applied. Survival curves were generated using the Kaplan-Meier method and compared via the log-rank test. A P value < 0.05 was considered statistically significant.

Results

scRNA-seq profiling reveals transcriptomic divergence between malignant and non-malignant epithelial cells

To characterize the cellular composition of LUAD, scRNA-seq was performed on a clinical cohort. Unsupervised clustering and UMAP visualization identified major cell lineages within the TME (Fig. 1a), with their identities validated by the expression of canonical marker genes (Fig. 1b). UMAP projections highlighted notable inter-patient heterogeneity (Fig. 1c) and a distinct redistribution of cell populations when comparing

tumor tissues with their normal counterparts (Fig. 1d).

To precisely define the malignant compartment within the epithelial lineage, inferCNV analysis was initially employed to assess chromosomal copy number variations. Epithelial cells derived from tumor tissues exhibited extensive genomic instability and large-scale CNV alterations compared to those from normal controls, providing robust genomic evidence for their malignant status (Fig. 1e). Following this identification, the malignant epithelial cells and non-malignant epithelial cells were visualized via UMAP, confirming a clear transcriptomic separation between the two groups (Fig. 1f). Based on this classification, differential expression analysis (DEA) was utilized to identify genes specifically enriched in the malignant population (Fig. 1h). These data establish a comprehensive landscape of the transcriptomic divergence between tumor and normal epithelial cells, providing a foundation for identifying key drivers of malignancy and subsequent therapeutic resistance in LUAD.

scRNA-seq characterization of malignant epithelial subclusters associated with chemo-immunotherapy resistance

To further investigate the cellular determinants of therapeutic response, scRNA-seq was performed on a clinical cohort comprising patients with distinct responses to chemo-immunotherapy. Unsupervised clustering identified major cell populations within the TME (Fig. 2a). When partitioned by clinical response, the UMAP visualization revealed a stable distribution of cell lineages between the responsive (R) and non-responsive (NR) groups (Fig. 2b), with each cluster validated by canonical marker genes (Fig. 2c).

To isolate the malignant driving forces, we confirmed the malignant state of all epithelial cells by inferCNV analysis (Fig. 2d). All epithelial cells were extracted and categorized into malignant and non-malignant compartments (Fig. 2e). Subsequent sub-clustering of these malignant cells yielded distinct sub-populations, designated C0 to C5 (Fig. 2f). Intriguingly, compositional analysis revealed that the C0 sub-cluster was markedly enriched in the NR group, whereas its proportion was significantly lower in the R group (Fig. 2g). This disparity suggests that the C0 sub-cluster may specifically

mediate the resistance of LUAD to combined chemo-immunotherapy, necessitating a more profound characterization of this specific cell population.

To define the functional identity of these sub-clusters, differential expression analysis was performed to identify lineage-specific markers (Fig. 2h). Notably, GSEA analysis revealed that the resistance-associated C0 sub-cluster was significantly enriched in genes related to oxidative phosphorylation (Fig. 2i). These transcriptomic features indicate that C0 cells possess a higher degree of malignancy and metabolic adaptation, which may support their survival under therapeutic stress. Moreover, the C0 sub-cluster score exhibited a significant positive correlation with the infiltration of regulatory T cells (Fig. 2j) and M2-polarized macrophages (Fig. 2k).

Collectively, these data identify the C0 sub-cluster as a pivotal orchestrator of chemo-immunotherapy resistance in LUAD.

Identification of SLC2A1 as a key driver of chemo-immunotherapy resistance in LUAD

Next, we sought to identify the specific molecular drivers responsible for these observed phenotypes based on previous findings. To this end, a multi-dimensional intersection analysis was performed using four distinct gene sets: DEGs between R and NR cancer cells, the C0 sub-cluster signature, tumor-enriched genes, and malignant-specific epithelial markers. Notably, SLC2A1 emerged as the unique candidate overlapping across all four datasets (Fig. 3a), suggesting its pivotal role in both malignancy and therapeutic resistance**.** Although SLC2A1 is a well-characterized glucose transporter, its functional involvement in the malignant epithelial compartment, specifically in orchestrating resistance to combined chemo-immunotherapy, has not been comprehensively explored.

To evaluate the clinical significance of this finding, we first extended our analysis to large-scale public cohorts. Consequently, survival analysis of the TCGA-LUAD dataset revealed that patients with elevated *SLC2A1* expression experienced significantly shorter overall survival compared to those with low expression (Fig. 3b), consistent with its reported role as a poor prognostic marker in solid tumors (Hantzsch-

Kuhn et al., 2025; Zheng et al., 2022). Furthermore, immunohistochemistry (IHC) staining from the HPA database demonstrated a marked upregulation of SLC2A1 protein in tumor tissues relative to normal lung tissues (Fig. 3c).

Therefore, to confirm whether this molecular feature directly correlates with clinical treatment outcomes, SLC2A1 levels were rigorously examined in our own patient samples. Western blot analysis exhibited a robust increase in SLC2A1 protein levels in the NR group compared to the R group (Fig. 3d). Moreover, this trend was further validated by IHC staining of clinical sections, which showed that the NR group possessed a significantly higher proportion of SLC2A1-positive malignant cells and greater staining intensity (Fig. 3e). In conclusion, these multi-level validations collectively identify SLC2A1 as a high-confidence driver of treatment failure, providing a solid clinical foundation for investigating its downstream signaling mechanisms in LUAD resistance.

SLC2A1 positively regulates the AKT signaling pathway in LUAD cells

Next, we further explored the downstream signaling mechanisms through which SLC2A1 exerts its functional effects. Notably, the AKT pathway was consistently identified as highly active in both $SLC2A1^{+}$ malignant cells and malignant cells from non-responsive patients (Fig. 4a, Supplementary Fig.1). Consistent with this finding, western blot analysis of patient samples confirmed that p-AKT levels were markedly elevated in the NR group (Fig. 4b). Consequently, we hypothesized that SLC2A1 might act as a functional upstream regulator of the AKT pathway, which is recognized as a master regulator of tumor growth and therapeutic evasion (Hassan et al., 2024; Jiang et al., 2025).

To test this hypothesis, we performed loss-of-function and gain-of-function experiments in A549 and H1299 cell lines. Specifically, silencing *SLC2A1* using small interfering RNAs (hereafter, si*SLC2A1*-1 and *SLC2A1*-2) led to a significant reduction in SLC2A1 protein levels (Fig. 4c, d). More importantly, this knockdown resulted in a substantial decrease in p-AKT levels in both cell lines, while the total AKT pool remained largely invariant (Fig. 4e, f).

Conversely, we established *SLC2A1*-overexpressing cell models (Hereafter, ov*SLC2A1*) to investigate if SLC2A1 is sufficient to drive AKT activation (Fig. 4g, h). As expected, the overexpression of SLC2A1 led to a robust increase in AKT phosphorylation in both A549 and H1299 cells (Fig. 4i, j). Notably, this upregulation occurred without a concomitant change in total AKT expression, confirming that SLC2A1 specifically modulates the phosphorylation status of the AKT pathway rather than its baseline expression. In summary, these results demonstrate a strong positive regulatory relationship between SLC2A1 and the AKT signaling axis, providing a mechanistic link to the therapeutic resistance observed in NR patients.

SLC2A1 promotes chemoresistance and malignant progression in LUAD cells

In accordance with our observations, si*SLC2A1*-1/2 significantly sensitized LUAD cells to chemotherapy treated with cisplatin. Specifically, in A549 cells, the IC_{50} of cisplatin dropped from 19.68 μM in the NC group to 6.068 μM and 8.256 μM in the knockdown groups (Fig. 5a). A similar trend was observed in H1299 cells, where the IC_{50} decreased from 26.20 μM to 10.45 μM and 12.77 μM upon SLC2A1 depletion (Fig. 5b). Conversely, ov*SLC2A1* conferred robust chemoresistance, as evidenced by the elevated IC_{50} values in both A549 (27.83 μM vs. 18.46 μM) and H1299 cells (38.37 μM vs. 25.97 μM) (Fig. 5c, d). Furthermore, the percentage of apoptotic cells increased significantly following SLC2A1 knockdown in both A549 (Fig. 5e) and H1299 lines (Fig. 5f). On the contrary, cells in the ov*SLC2A1* group were markedly protected from cisplatin-induced apoptosis, exhibiting a substantial reduction in apoptotic rates compared to the control (Fig. 5g, h). These results collectively suggest that SLC2A1 is a critical mediator of chemoresistance by inhibiting apoptosis. In addition, transwell migration assays revealed that si*SLC2A1*-1/2 led to a remarkable decrease in the relative migration rate of both cell lines (Fig. 5i, j). In sharp contrast, ov*SLC2A1* significantly augmented migratory capacity, with the relative migration rate nearly doubling in both A549 and H1299 cells (Fig. 5k, l). Therefore, these functional findings demonstrate that SLC2A1 not only drives therapeutic resistance but also promotes the aggressive metastatic phenotype of LUAD cells.

The AKT axis is essential for SLC2A1-mediated chemo-immunotherapy resistance

Given the correlation between SLC2A1 and malignancy, we investigated whether its effects depend on downstream AKT signaling. To this end, rescue experiments using the AKT inhibitor MK-2206 were conducted to verify the AKT axis as the critical mediator of SLC2A1-driven resistance. Notably, the increased resistance to cisplatin induced by ov*SLC2A1* was significantly abrogated upon the addition of MK-2206 in A549 cells, with the IC_{50} of cisplatin dropping from 29.11 μM in the ov*SLC2A1* group to 11.11 μM after AKT inhibition (Fig. 6a). Similarly, MK-2206 reduced the IC_{50} from 37.98 μM to 18.07 μM in H1299 cells (Fig. 6b). Furthermore, flow cytometry confirmed that the anti-apoptotic effect of SLC2A1 was effectively neutralized by MK-2206, leading to a marked increase in the proportion of apoptotic cells in both A549 (Fig. 6c) and H1299 lines (Fig. 6d). Moreover, aligning with our previous findings, transwell assays showed that ov*SLC2A1*-induced migration was significantly enhanced, yet this effect was substantially reversed by MK-2206 (Fig. 6e, f). More importantly, we examined the expression of PD-L1, a key checkpoint for immune refractoriness. Intriguingly, the expression of PD-L1 markedly reduced when SLC2A1 was silenced in both A549 (Fig. 6g) and H1299 lines (Fig. 6h). In contrast, while ov*SLC2A1* led to a robust upregulation of surface PD-L1, this effect was almost entirely abolished by MK-2206 treatment (Fig. 6i, j). This directly supports the AKT pathway as the critical link between SLC2A1 and PD-L1 mediated immune escape, a mechanism supported by previous studies showing that AKT activation is a master driver of PD-L1 stabilization and synthesis(Lastwika et al., 2016; Quan et al., 2022).

In conclusion, these results provide definitive evidence that the AKT signaling axis is the indispensable pathway through which SLC2A1 coordinates both chemoresistance and PD-L1 mediated immunotherapy resistance in LUAD.

Discussion

The clinical management of LUAD has transitioned into a new era characterized

by the integration of platinum-based chemotherapy and PD-1/PD-L1 blockade. Despite these advances, resistance to combined therapy continues to undermine durable survival benefits. In this study, we applied scRNA-seq to clinical LUAD specimens in an effort to dissect the cellular composition underlying treatment failure. Rather than relying solely on bulk transcriptomic signals, this approach allowed us to resolve intra-tumoral heterogeneity at single-cell resolution. Through this analysis, we identified a malignant subpopulation that was markedly enriched in non-responders.

Building on this observation, we found that SLC2A1 was highly expressed within this resistance-associated cluster. SLC2A1 is conventionally described as a facilitative glucose transporter that sustains aerobic glycolysis in cancer cells. However, our data suggest that its contribution to therapy resistance extends beyond metabolic reprogramming. Specifically, we observed that SLC2A1 functions as a non-canonical signaling scaffold, a membrane-associated organizer of signaling complexes potentially beyond its canonical transport capacity, to maintain AKT activation. Persistent AKT phosphorylation then supports two resistance-related processes: attenuation of cisplatin-induced apoptosis and stabilization of PD-L1 expression. From this angle, SLC2A1 appears to coordinate survival signaling and immune checkpoint regulation within the same molecular context, rather than acting through isolated pathways.

Through this study, our findings provide a framework for understanding chemo-immunotherapy resistance beyond isolated mechanisms. Historically, resistance to chemotherapy and resistance to immunotherapy in LUAD have been examined as parallel but distinct phenomena. Chemotherapy resistance is frequently attributed to bypass pathway activation, such as MET amplification or PI3K hyperactivation, which compensates for DNA damage-induced stress (Ashrafi et al., 2022). In contrast, immunotherapy failure has often been linked to TME remodeling, including impaired antigen presentation or T cell exclusion (Wu et al., 2024). While each explanation is mechanistically sound, neither fully captures the clinical reality that dual resistance often develops in a coordinated manner. It is worth noting that interventions targeting a single pathway frequently result in rapid compensatory adaptation (Wang et al., 2025;

Xiang et al., 2024). Our findings raise the possibility that SLC2A1-driven AKT signaling may function as one such convergent hub, reducing the need for multiple independent resistance events. In this model, sustained AKT activity simultaneously preserves anti-apoptotic signaling and enhances PD-L1 stability.

With a clearer understanding of this integrated signaling axis, these findings may inform strategies to treat resistant tumors by specifically disrupting the non-canonical scaffold functions of SLC2A1. Historically, both SLC2A1 and AKT have been independently implicated in the orchestration of therapeutic failure across various malignancies. AKT, as a central node in the PI3K/AKT/mTOR pathway, has long been established as a master switch for cell survival, where its hyperactivation promotes DNA damage repair and inhibits pro-apoptotic proteins, directly leading to platinum-based chemotherapy resistance (Liu et al., 2020). Similarly, SLC2A1 has been extensively documented as a biomarker of high-grade malignancy; however, traditional research has predominantly focused on its metabolic role.

The innovation of our work, suggesting that SLC2A1 may function as a non-canonical upstream organizer of AKT activation. In our study, loss-of-function assays demonstrated that silencing SLC2A1 directly led to a significant reduction in AKT phosphorylation in A549 and H1299 cells, without altering total AKT levels. This suggests that SLC2A1 is essential for maintaining the activated state of this signaling axis. Conversely, ov*SLC2A1* showed that SLC2A1 was sufficient to trigger robust AKT phosphorylation, which functionally manifested as a dramatic increase in the IC_{50} of cisplatin. Most crucially, our rescue experiments using the AKT inhibitor MK-2206 provided supportive evidence that the oncogenic effects of SLC2A1 are mediated via this signaling scaffold. We observed that the enhanced migratory potential and the anti-apoptotic phenotype driven by SLC2A1 overexpression were almost entirely abrogated upon AKT inhibition. Furthermore, while AKT is known to regulate PD-L1 stability, our study is the first to identify SLC2A1 as a specific membrane recruiter that initiates this process under chemo-immunotherapy pressure. This finding suggests that SLC2A1 may be involved in the membrane-associated regulation of PD-L1. This finding aligns

with the emerging transceptor paradigm, where solute carriers sense extracellular stressors to activate intracellular kinase cascades. By linking SLC2A1 directly to the AKT/PD-L1 checkpoint, we provide a holistic view of tumor adaptation that justifies the use of AKT inhibitors as potent sensitizing agents for chemo-immunotherapy resistant LUAD.

Consequently, through translating these mechanistic insights into clinical practice, these insights may support patient stratification by addressing the escalating socio-economic burden of treatment failure. As refractory disease necessitates transitions to costly and frequently ineffective second-line interventions (Courtney et al., 2021), our identification of SLC2A1 as a high-confidence driver provides a critical window for patient stratification. Utilizing SLC2A1 as a predictive biomarker allows clinicians to spare non-responsive patients the toxicity of ineffective protocols, while identifying those who might benefit from adjunctive AKT-targeted therapies (Hao et al., 2025; Turner et al., 2023). Such precision strategies optimize survival outcomes and ensure the sustainable allocation of healthcare resources by aligning high-cost immunotherapies with the most receptive biological profiles.

Several limitations should be acknowledged. Although our conclusions are supported by cell line models and patient-derived samples, further validation in organoid systems or in vivo models would strengthen translational relevance. In addition, the precise molecular mechanism by which SLC2A1 sustains AKT phosphorylation remains undefined. Whether this involves direct interaction with PI3K, modulation of membrane lipid microdomains, or recruitment of adaptor proteins remains to be clarified. Future structural and proteomic studies will be necessary to resolve these questions.

Conclusion

In summary, our findings identify SLC2A1 as a previously underrecognized contributor to chemo-immunotherapy resistance in LUAD. Beyond its established role in glucose transport, SLC2A1 may function as an upstream signaling modulator that

sustains AKT activation and facilitates both cisplatin tolerance and PD-L1 mediated immune escape. By integrating survival signaling and immune checkpoint control within a shared molecular axis, the SLC2A1-AKT-PD-L1 pathway may represent an important contributor to therapeutic responsiveness. Targeting this node may therefore represent a rational strategy to overcome dual resistance and improve long-term outcomes in LUAD.

Acknowledgements

Not applicable.

Disclosures and declarations

Author contributions

Study concept and design: JSR: Conceptualization; Methodology; Investigation; Data curation; Formal analysis; Writing-original draft; Writing-review & editing; Funding acquisition. MXZ: Conceptualization; Methodology; Investigation; Data curation; Formal analysis; Writing-original draft; Writing-review & editing. YY: Conceptualization; Methodology; Formal analysis; Writing-review & editing; Supervision. JLZ: Conceptualization; Methodology; Formal analysis; Writing-review & editing; Supervision. All authors have read and approved the final manuscript.

Funding

This research was supported by youth research project funded by the Jinshan District Health Commission and Science and Technology Commission (No. JSKJ-KTQN-2024-03).

Data availability

The datasets presented in this study can be found in online public repositories. The names of the repositories, accession numbers and original contributions presented in

the study can be found in the article.

Ethical approval statement

This study was conducted in accordance with the Declaration of Helsinki and was approved by the Institutional Ethics Committee of Jinshan Hospital of Fudan University (Approval No. JIEC 2025-S32). The participants provided written informed consent to participate in this study.

Clinical trial number

Not applicable.

References

Ashrafi, A., Akter, Z., Modareszadeh, P., Modareszadeh, P., Berisha, E., Alemi, P.S.*, et al.* (2022). Current Landscape of Therapeutic Resistance in Lung Cancer and Promising Strategies to Overcome Resistance. Cancers *14*.https://doi.org/10.3390/cancers14194562.

Courtney, P.T., Yip, A.T., Cherry, D.R., Salans, M.A., Kumar, A., and Murphy, J.D. (2021). Cost-effectiveness of Nivolumab-Ipilimumab Combination Therapy for the Treatment of Advanced Non-Small Cell Lung Cancer. JAMA network open *4*, e218787.https://doi.org/10.1001/jamanetworkopen.2021.8787.

Gao, Y., Feng, Y., Liu, S., Zhang, Y., Wang, J., Qin, T.*, et al.* (2023). Immune-independent acquired resistance to PD-L1 antibody initiated by PD-L1 upregulation via PI3K/AKT signaling can be reversed by anlotinib. Cancer medicine *12*, 15337-15349.https://doi.org/10.1002/cam4.6195.

Hantzsch-Kuhn, B., Schraps, N., Reck, M., von Weihe, S., Olchers, T., Ellebrecht, D.B.*, et al.* (2025). High GLUT1 protein expression is associated with unfavorable tumor features and poor prognosis in non-small cell lung cancer. Translational lung cancer research *14*, 4838-4848.https://doi.org/10.21037/tlcr-2025-422.

Hao, C., Wei, Y., Meng, W., Zhang, J., and Yang, X. (2025). PI3K/AKT/mTOR

inhibitors for hormone receptor-positive advanced breast cancer. Cancer treatment reviews *132*, 102861.https://doi.org/10.1016/j.ctrv.2024.102861.

Hassan, D., Menges, C.W., Testa, J.R., and Bellacosa, A. (2024). AKT kinases as therapeutic targets. Journal of experimental & clinical cancer research : CR *43*, 313.https://doi.org/10.1186/s13046-024-03207-4.

Huang, Q., Li, Y., Huang, Y., Wu, J., Bao, W., Xue, C.*, et al.* (2025). Advances in molecular pathology and therapy of non-small cell lung cancer. Signal transduction and targeted therapy *10*, 186.https://doi.org/10.1038/s41392-025-02243-6.

Jiang, M., Zhang, K., Zhang, Z., Zeng, X., Huang, Z., Qin, P.*, et al.* (2025). PI3K/AKT/mTOR Axis in Cancer: From Pathogenesis to Treatment. MedComm *6*, e70295.https://doi.org/10.1002/mco2.70295.

Kessler, J.E., Park, K.N., Grizzle, A.J., and Hurwitz, J.T. (2023). Cost of illness of stage IV non-small cell lung cancer (NSCLC) positive for programmed cell death ligand 1 (PD-L1) in the US. Expert review of pharmacoeconomics & outcomes research *23*, 55-61.https://doi.org/10.1080/14737167.2023.2140141.

Lahiri, A., Maji, A., Potdar, P.D., Singh, N., Parikh, P., Bisht, B.*, et al.* (2023). Lung cancer immunotherapy: progress, pitfalls, and promises. Molecular cancer *22*, 40.https://doi.org/10.1186/s12943-023-01740-y.

Lastwika, K.J., Wilson, W., 3rd, Li, Q.K., Norris, J., Xu, H., Ghazarian, S.R.*, et al.* (2016). Control of PD-L1 Expression by Oncogenic Activation of the AKT-mTOR Pathway in Non-Small Cell Lung Cancer. Cancer research *76*, 227-238.https://doi.org/10.1158/0008-5472.Can-14-3362.

Laughney, A.M., Hu, J., Campbell, N.R., Bakhoum, S.F., Setty, M., Lavallée, V.P.*, et al.* (2020). Regenerative lineages and immune-mediated pruning in lung cancer metastasis. Nature medicine *26*, 259-269.https://doi.org/10.1038/s41591-019-0750-6.

Li, J., Hu, J., Yang, Y., Zhang, H., Liu, Y., Fang, Y.*, et al.* (2025). Drug resistance in cancer: molecular mechanisms and emerging treatment strategies. Molecular biomedicine *6*, 111.https://doi.org/10.1186/s43556-025-00352-w.

Liu, R., Chen, Y., Liu, G., Li, C., Song, Y., Cao, Z.*, et al.* (2020). PI3K/AKT pathway as a key link modulates the multidrug resistance of cancers. Cell death & disease *11*, 797.https://doi.org/10.1038/s41419-020-02998-6.

Memon, D., Schoenfeld, A.J., Ye, D., Fromm, G., Rizvi, H., Zhang, X.*, et al.* (2024). Clinical and molecular features of acquired resistance to immunotherapy in non-small cell lung cancer. Cancer cell *42*, 209-224.e209.https://doi.org/10.1016/j.ccell.2023.12.013.

Meyer, M.L., Fitzgerald, B.G., Paz-Ares, L., Cappuzzo, F., Jänne, P.A., Peters, S.*, et al.* (2024). New promises and challenges in the treatment of advanced non-small-cell lung cancer. Lancet (London, England) *404*, 803-822.https://doi.org/10.1016/s0140-6736(24)01029-8.

Quan, Z., Yang, Y., Zheng, H., Zhan, Y., Luo, J., Ning, Y.*, et al.* (2022). Clinical implications of the interaction between PD-1/PD-L1 and PI3K/AKT/mTOR pathway in progression and treatment of non-small cell lung cancer. Journal of Cancer *13*, 3434-3443.https://doi.org/10.7150/jca.77619.

Siegel, R.L., Miller, K.D., Fuchs, H.E., and Jemal, A. (2021). Cancer Statistics, 2021. CA: a cancer journal for clinicians *71*, 7-33.https://doi.org/10.3322/caac.21654.

Tufail, M., Jiang, C.H., and Li, N. (2025). Immune evasion in cancer: mechanisms and cutting-edge therapeutic approaches. Signal transduction and targeted therapy *10*, 227.https://doi.org/10.1038/s41392-025-02280-1.

Turner, N.C., Oliveira, M., Howell, S.J., Dalenc, F., Cortes, J., Gomez Moreno, H.L.*, et al.* (2023). Capivasertib in Hormone Receptor-Positive Advanced Breast Cancer. The New England journal of medicine *388*, 2058-2070.https://doi.org/10.1056/NEJMoa2214131.

Wang, H., Niu, X., Jin, Z., Zhang, S., Fan, R., Xiao, H.*, et al.* (2025). Immunotherapy resistance in non-small cell lung cancer: from mechanisms to therapeutic opportunities. Journal of experimental & clinical cancer research : CR *44*, 250.https://doi.org/10.1186/s13046-025-03519-z.

Watterson, A., and Coelho, M.A. (2023). Cancer immune evasion through KRAS and PD-L1 and potential therapeutic interventions. Cell communication and signaling :

CCS *21*, 45.https://doi.org/10.1186/s12964-023-01063-x.

Wu, B., Zhang, B., Li, B., Wu, H., and Jiang, M. (2024). Cold and hot tumors: from molecular mechanisms to targeted therapy. Signal transduction and targeted therapy *9*, 274.https://doi.org/10.1038/s41392-024-01979-x.

Xiang, Y., Liu, X., Wang, Y., Zheng, D., Meng, Q., Jiang, L.*, et al.* (2024). Mechanisms of resistance to targeted therapy and immunotherapy in non-small cell lung cancer: promising strategies to overcoming challenges. Frontiers in immunology *15*, 1366260.https://doi.org/10.3389/fimmu.2024.1366260.

Xu, Y., Shen, H., Shang, D., and Zhu, C. (2025). Pharmacological strategies to overcome immune checkpoint inhibitor resistance in non-small cell lung cancer. Frontiers in oncology *15*, 1665239.https://doi.org/10.3389/fonc.2025.1665239.

Yan, Y., Sun, D., Hu, J., Chen, Y., Sun, L., Yu, H.*, et al.* (2025). Multi-omic profiling highlights factors associated with resistance to immuno-chemotherapy in non-small-cell lung cancer. Nature genetics *57*, 126-139.https://doi.org/10.1038/s41588-024-01998-y.

Yang, M., Cui, M., Sun, Y., Liu, S., and Jiang, W. (2024). Mechanisms, combination therapy, and biomarkers in cancer immunotherapy resistance. Cell communication and signaling : CCS *22*, 338.https://doi.org/10.1186/s12964-024-01711-w.

Zheng, H., Long, G., Zheng, Y., Yang, X., Cai, W., He, S.*, et al.* (2022). Glycolysis-Related SLC2A1 Is a Potential Pan-Cancer Biomarker for Prognosis and Immunotherapy. Cancers *14*.https://doi.org/10.3390/cancers14215344.

Figure Legends

Fig. 1 scRNA-seq profiling reveals the transcriptomic landscape and identification of malignant cells in LUAD. (a) UMAP visualization identifying major cell lineages within the TME across the clinical cohort; (b) Dot plot showing the expression of canonical marker genes used to validate the identity of each cell lineage; (c) UMAP projection of the integrated scRNA-seq dataset colored by patient origin; (d) Comparative UMAP analysis demonstrating the redistribution of cell populations between tumor tissues and matched normal counterparts; (e) InferCNV analysis depicting large-scale chromosomal CNV alterations in epithelial cells to confirm the malignant status of tumor-derived clusters; (f) UMAP plot highlighting the distinct transcriptomic separation between malignant and non-malignant epithelial cells; (g) DEA identifying key genes specifically enriched in the malignant epithelial population compared to normal controls. scRNA-seq: Single-cell RNA sequencing, LUAD: Lung adenocarcinoma, UMAP: Uniform Manifold Approximation and Projection, TME: Tumor microenvironment, CNV: Copy number variation, inferCNV: Inferring chromosomal copy number variation, DEA: Differential expression analysis.

Fig. 2 scRNA-seq characterization of malignant epithelial subclusters associated with chemo-immunotherapy resistance. (a) UMAP visualization identifying major cell populations within the TME of the scRNA-seq data of Yan et al.; (b) UMAP projections partitioned by clinical response, showing the distribution of cell lineages in R and NR groups; (c) Dot plot of canonical marker genes validating the identity of each cluster; (d) InferCNV analysis confirming the malignant nature of epithelial cells compared to diploid references; (e) UMAP plot categorizing epithelial cells into malignant and non-malignant compartments; (f) Sub-clustering of malignant epithelial cells identifying distinct sub-populations, designated C0 to C5; (g) Relative proportions of malignant sub-clusters in R and NR groups, highlighting the enrichment of the C0 sub-cluster in non-responsive patients; (h) Heatmap of DEA showing lineage-specific marker genes for each malignant sub-cluster; (i) GSEA plot revealing significant enrichment of oxidative phosphorylation pathways in the resistance-associated C0 sub-

cluster; (j, k) Correlation analysis showing the positive relationship between the C0 sub-cluster score and the infiltration of Tregs (J) and M2 macrophages (K). scRNA-seq: Single-cell RNA sequencing, LUAD: Lung adenocarcinoma, TME: Tumor microenvironment, UMAP: Uniform Manifold Approximation and Projection, R: Responsive, NR: Non-responsive, inferCNV: Inferring chromosomal copy number variation, DEA: Differential expression analysis, GSEA: Gene set enrichment analysis, Tregs: Regulatory T cells, M2: M2-polarized macrophages.

Fig. 3 Identification of SLC2A1 as a key driver of chemo-immunotherapy resistance in LUAD. (a) Venn diagram illustrating the multi-dimensional intersection analysis of four gene sets: DEGs (R vs. NR), C0 sub-cluster signature, tumor-enriched genes (from epithelial cells), and malignant-specific epithelial markers, identifying SLC2A1 as the sole overlapping candidate; (b) Kaplan-Meier survival analysis from the TCGA-LUAD dataset showing the correlation between high SLC2A1 expression and shortened overall survival; (c) Representative IHC images from the HPA database comparing SLC2A1 protein levels in normal lung tissues versus tumor tissues; (d) Western blot analysis and corresponding quantification of SLC2A1 protein expression in clinical samples from the R and NR groups; (e) Representative IHC images and statistical analysis of IHC scores for SLC2A1 in our clinical cohort, comparing responsive and non-responsive patients. SLC2A1: Solute Carrier Family 2 Member 1 LUAD: Lung adenocarcinoma DEGs: Differentially expressed genes R: Responsive NR: Non-responsive TCGA: The Cancer Genome Atlas IHC: Immunohistochemistry HPA: Human Protein Atlas. Student's t-test was used to compare two groups, while one-way ANOVA followed by Tukey's post hoc test was used for comparisons between three or more groups. * $p < 0.05$; ** $p < 0.01$; **** $p < 0.0001$.

Fig. 4 SLC2A1 positively regulates the AKT signaling pathway in LUAD cells. (a) GSEA plots and enrichment analysis showing the activation of the AKT signaling pathway in SLC2A1^{+} malignant cells and cells from the NR group from Yan's data; (b) Western blot analysis of clinical samples demonstrating elevated p-AKT levels in NR

patients compared to R patients; (c, d) Western blot validation of SLC2A1 knockdown efficiency using two independent siRNAs (si*SLC2A1*-1 and si*SLC2A1*-2) in A549 and H1299 cell lines; (e, f) Western blot analysis showing that silencing SLC2A1 results in a significant reduction of p-AKT levels while total AKT remains unchanged; (g, h) Western blot validation of SLC2A1 protein levels in A549 and H1299 cells following stable transduction with ov*SLC2A1* vectors; (i, j) Western blot analysis demonstrating that overexpression of SLC2A1 is sufficient to drive a robust increase in p-AKT levels without altering total AKT baseline expression. SLC2A1: Solute Carrier Family 2 Member 1, LUAD: Lung adenocarcinoma, AKT: Protein Kinase B, p-AKT: Phosphorylated AKT, GSEA: Gene set enrichment analysis, NR: Non-responsive R: Responsive, siRNA: Small interfering RNA, ov*SLC2A1*: SLC2A1 overexpression. Student's t-test was used to compare two groups, while one-way ANOVA followed by Tukey's post hoc test was used for comparisons between three or more groups. * $p <$ 0.05; ** $p < 0.01$; *** $p < 0.001$; **** $p < 0.0001$.

Fig. 5 SLC2A1 promotes chemoresistance and malignant progression in LUAD cells. (a, b) CCK-8 assays showing the IC_{50} values of cisplatin in A549 and H1299 cells following si*SLC2A1*-1/2 mediated knockdown compared to the NC group; (c, d) CCK-8 assays demonstrating the shift in IC_{50} values of cisplatin in A549 and H1299 cells overexpressing SLC2A1 (ov*SLC2A1*); (e, f) Flow cytometry analysis and quantification of apoptotic rates in SLC2A1-silenced A549 and H1299 cells under cisplatin treatment; (g, h) Flow cytometry analysis showing the inhibitory effect of ov*SLC2A1* on cisplatin-induced apoptosis; (i, j) Representative images and quantification of Transwell migration assays in A549 and H1299 cells after SLC2A1 knockdown; (k, l) Transwell migration assays demonstrating the increased migratory capacity of A549 and H1299 cells following stable ov*SLC2A1* transduction. SLC2A1: Solute Carrier Family 2 Member 1, LUAD: Lung adenocarcinoma, IC_{50}: Half-maximal inhibitory concentration, si*SLC2A1*: Small interfering RNA targeting SLC2A1, NC: Negative control, ov*SLC2A1*: SLC2A1 overexpression. Student's t-test was used to compare two groups, while one-way ANOVA followed by Tukey's post hoc test was used for comparisons

between three groups. *** $p < 0.001$; **** $p < 0.0001$.

Fig. 6 The AKT axis is essential for SLC2A1-mediated chemo-immunotherapy resistance. (a, b) CCK-8 assays demonstrating that the increased IC_{50} of cisplatin induced by ov*SLC2A1* is significantly abrogated following treatment with the AKT inhibitor MK-2206 in A549 and H1299 cells; (c, d) Flow cytometry analysis and quantification showing that the anti-apoptotic effect of SLC2A1 is neutralized by MK-2206, leading to a marked recovery of apoptotic rates; (e, f) Transwell migration assays and statistical analysis revealing that MK-2206 successfully reverses the enhanced migratory capacity driven by ov*SLC2A1*; (g, h) Flow cytometry analysis of surface PD-L1 expression, demonstrating that the marked downregulation of PD-L1 induced by SLC2A1 silencing in A549 and H1299 cells; (i, j) Flow cytometry analysis of surface PD-L1 expression, demonstrating that the robust upregulation of PD-L1 induced by ov*SLC2A1* is abolished upon AKT inhibition. IC_{50}: Half-maximal inhibitory concentration, LUAD: Lung adenocarcinoma, SLC2A1: Solute Carrier Family 2 Member 1, MK-2206: A highly selective allosteric AKT inhibitor, ov*SLC2A1*: SLC2A1 overexpression. Student's t-test was used to compare two groups, while one-way ANOVA followed by Tukey's post hoc test was used for comparisons between three groups. ** $p < 0.01$; *** $p < 0.001$; **** $p < 0.0001$.

Figure 1

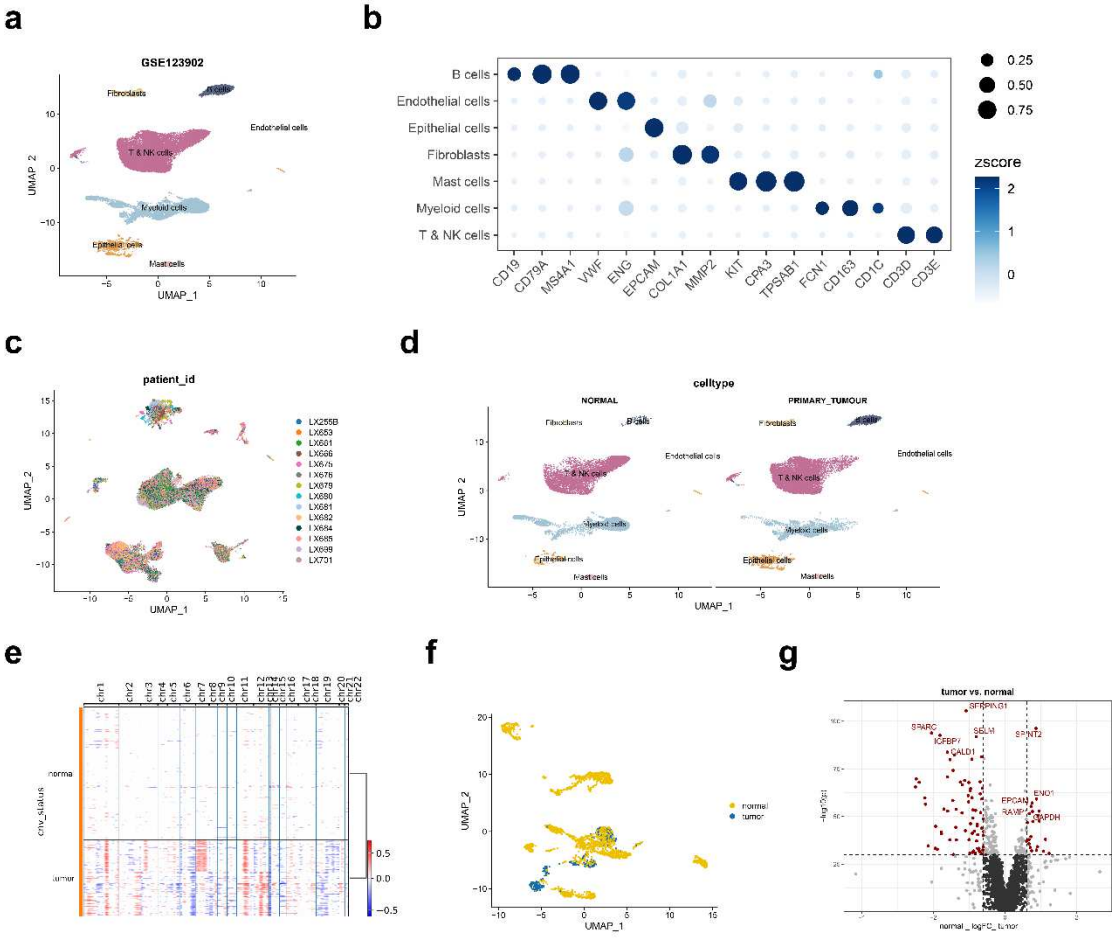

a
GSE123902
Fibroblasts
Endothelial cells
T & NK cells
Myeloid cells
Epithelial cells
Mast cells
UMAP_1
UMAP_2
b
B cells
Endothelial cells
Epithelial cells
Fibroblasts
Mast cells
Myeloid cells
T & NK cells
CD19
CD79A
MS4A1
VWF
ENG
EPCAM
COL1A1
MMP2
KIT
CPA3
TPSAB1
FCN1
CD163
CD1C
CD3D
CD3E
0.25
0.50
0.75
zscore
2
1
0
c
patient_id
LX255B
LX653
LX601
LX666
LX676
LX675
LX679
LX680
LX681
LX682
LX684
LX685
LX699
LX701
UMAP_1
UMAP_2
d
celltype
NORMAL
PRIMARY_TUMOUR
Fibroblasts
B cells
Endothelial cells
T & NK cells
Myeloid cells
Epithelial cells
Mast cells
UMAP_1
UMAP_2
e
chr1
chr2
chr3
chr4
chr5
chr6
chr7
chr8
chr9
chr10
chr11
chr12
chr13
chr14
chr15
chr16
chr17
chr18
chr19
chr20
chr21
chr22
cnv_status
normal
tumor
0.5
0.0
−0.5
f
UMAP_1
UMAP_2
normal
tumor
g
tumor vs. normal
SFRP4
SPARC
ICFBP7
GALD1
SELM
SPINT2
EPCAM
RAMP1
ENO1
GAPDH
-log10p1
normal_logFC_tumor

Figure 2

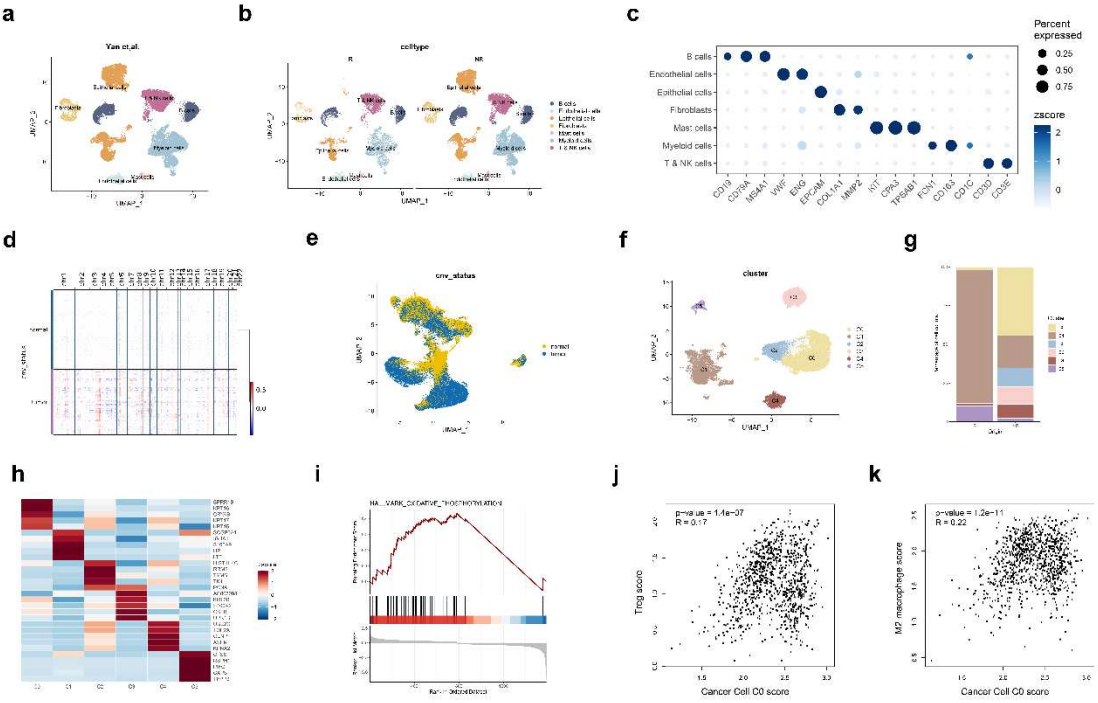

a
b
c
d
e
f
g
h
i
j
k
Yan et.al.
celltype
R
NR
Percent expressed
0.25
0.50
0.75
zscore
B cells
Endothelial cells
Epithelial cells
Fibroblasts
Mast cells
Myeloid cells
T & NK cells
CD19
CD79A
MS4A1
VWF
ENG
EPCAM
COL1A1
MMP2
KIT
CPA3
TPSAB1
FCN1
CD163
CD1C
CD3D
CD3E
cnv_status
cluster
Treg score
Cancer Cell C0 score
M2 macrophage score
Cancer Cell C0 score

Figure 3

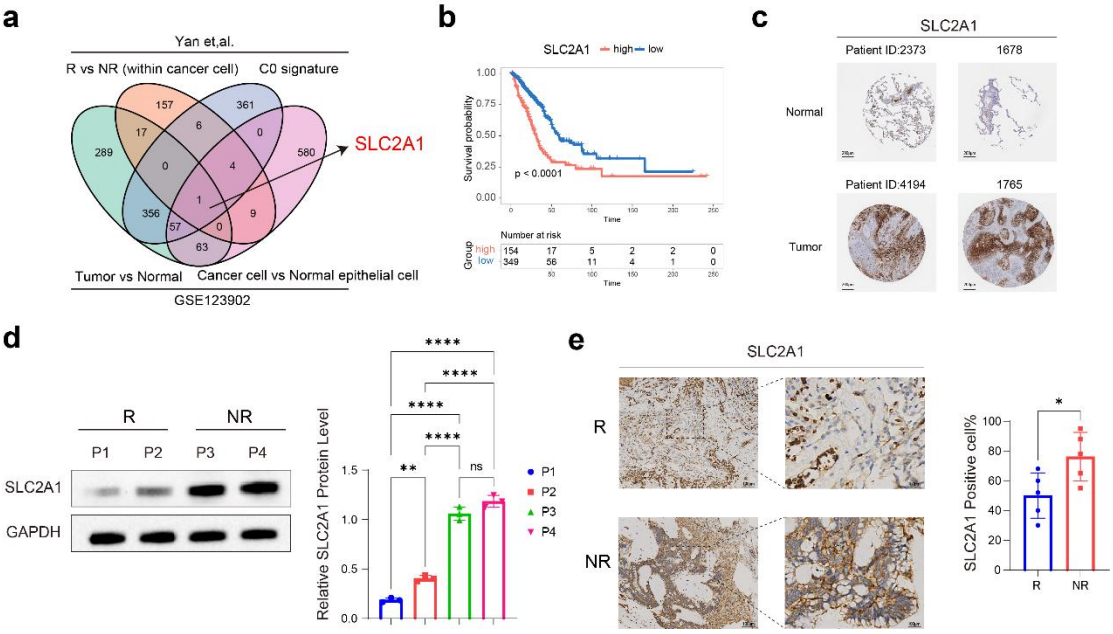

a
Yan et,al.
R vs NR (within cancer cell)
C0 signature
157
361
17
6
0
289
0
4
580
SLC2A1
1
356
57
0
9
63
Tumor vs Normal
Cancer cell vs Normal epithelial cell
GSE123902
b
SLC2A1 high low
Survival probability
p < 0.0001
Time
Number at risk
Group
high 154 17 5 2 2 0
low 349 56 11 4 1 0
c
SLC2A1
Patient ID:2373
1678
Normal
Patient ID:4194
1765
Tumor
d
R
NR
P1
P2
P3
P4
SLC2A1
GAPDH
Relative SLC2A1 Protein Level
****
**
ns
e
SLC2A1
R
NR
SLC2A1 Positive cell%
*

Figure 4

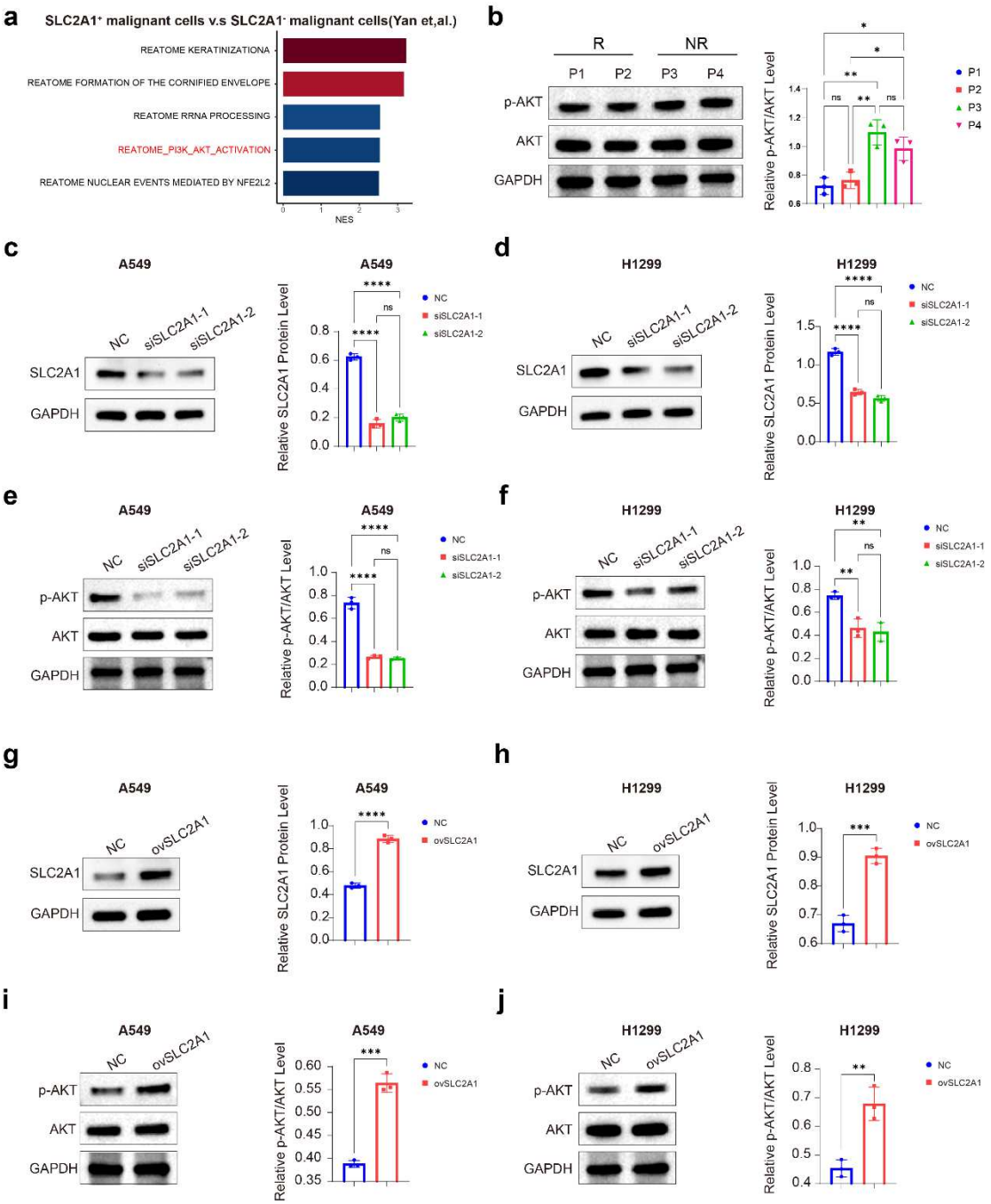

a
SLC2A1+ malignant cells v.s SLC2A1- malignant cells(Yan et,al.)
REATOME KERATINIZATIONA
REATOME FORMATION OF THE CORNIFIED ENVELOPE
REATOME RRNA PROCESSING
REATOME_PI3K_AKT_ACTIVATION
REATOME NUCLEAR EVENTS MEDIATED BY NFE2L2
NES
b
R
NR
P1
P2
P3
P4
p-AKT
AKT
GAPDH
Relative p-AKT/AKT Level
c
A549
NC
siSLC2A1-1
siSLC2A1-2
SLC2A1
GAPDH
Relative SLC2A1 Protein Level
d
H1299
e
p-AKT
AKT
Relative p-AKT/AKT Level
f
g
ovSLC2A1
h
i
j

Figure 5

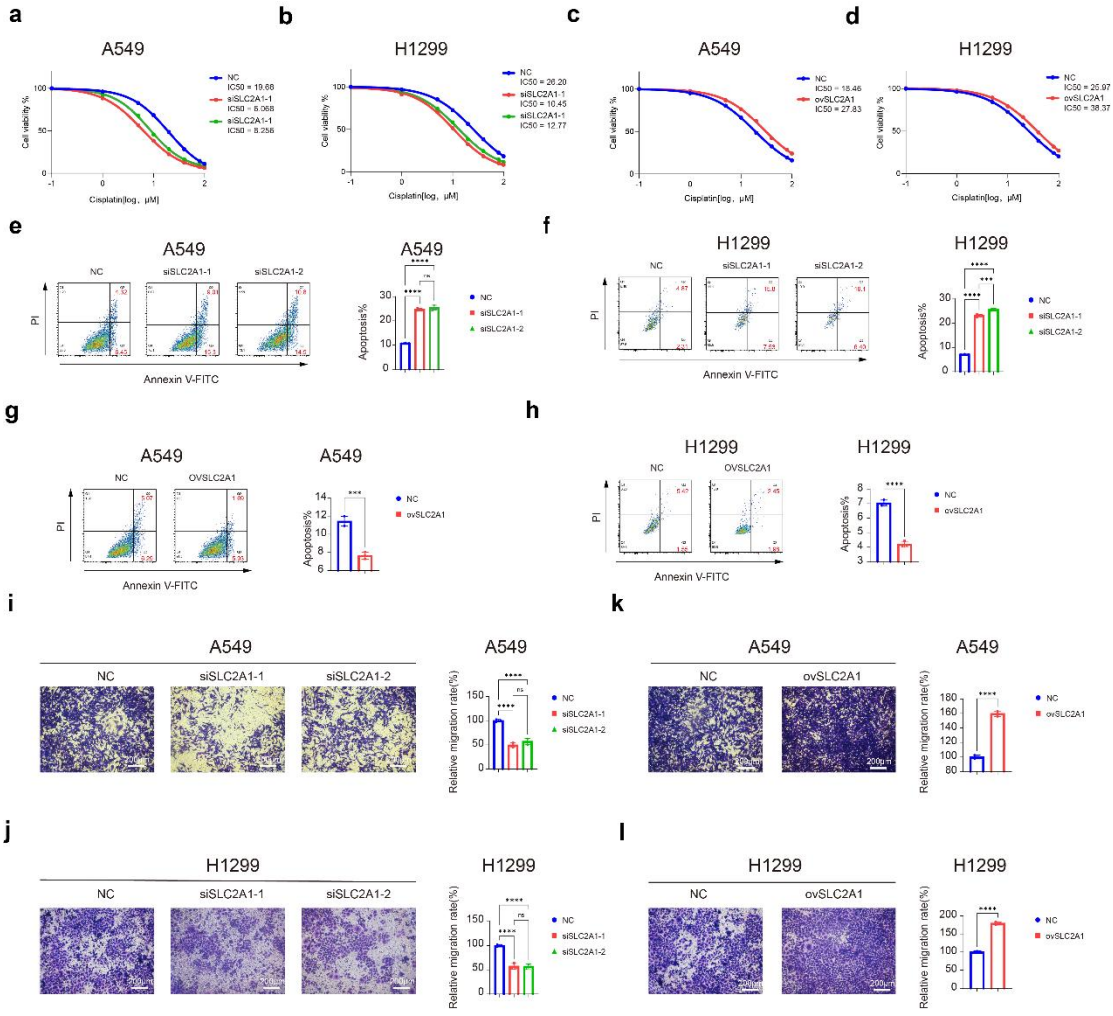
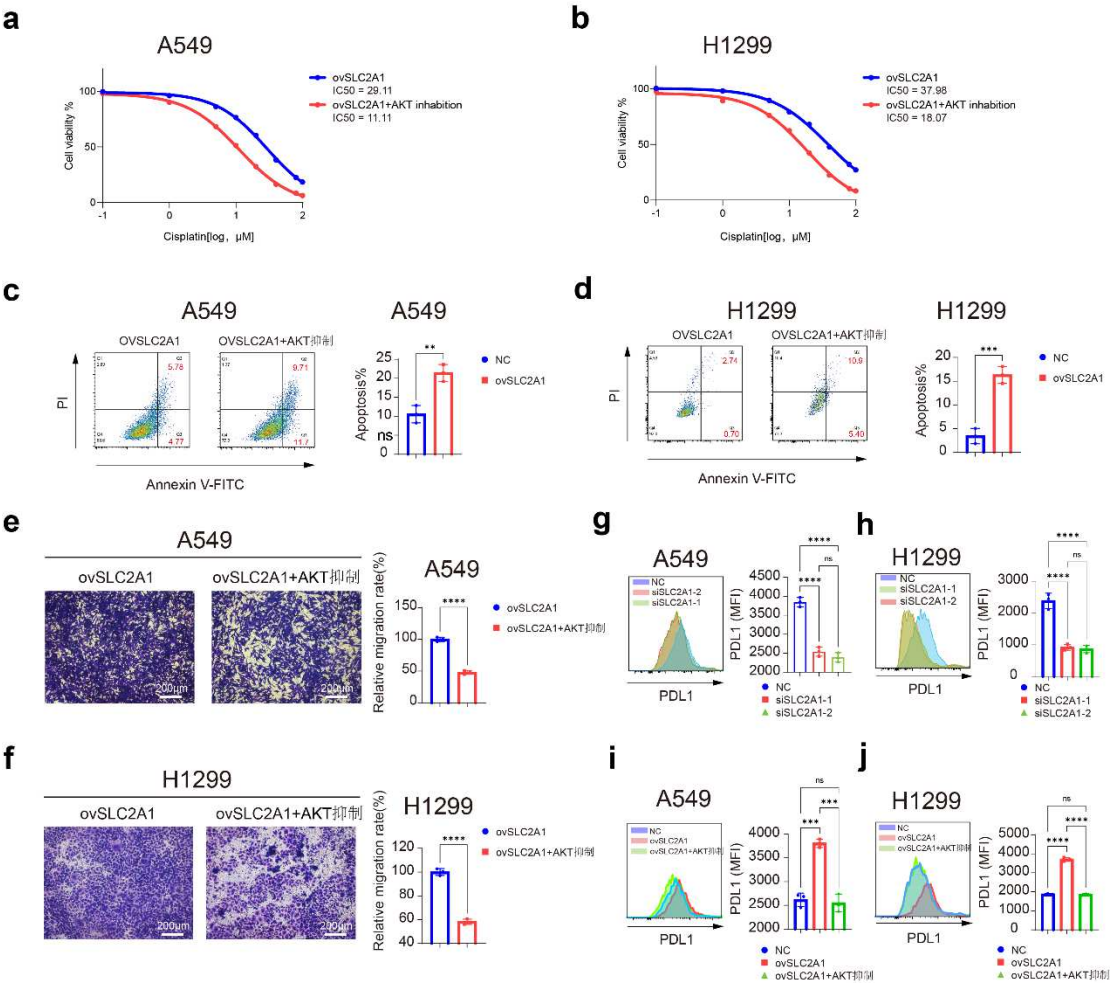
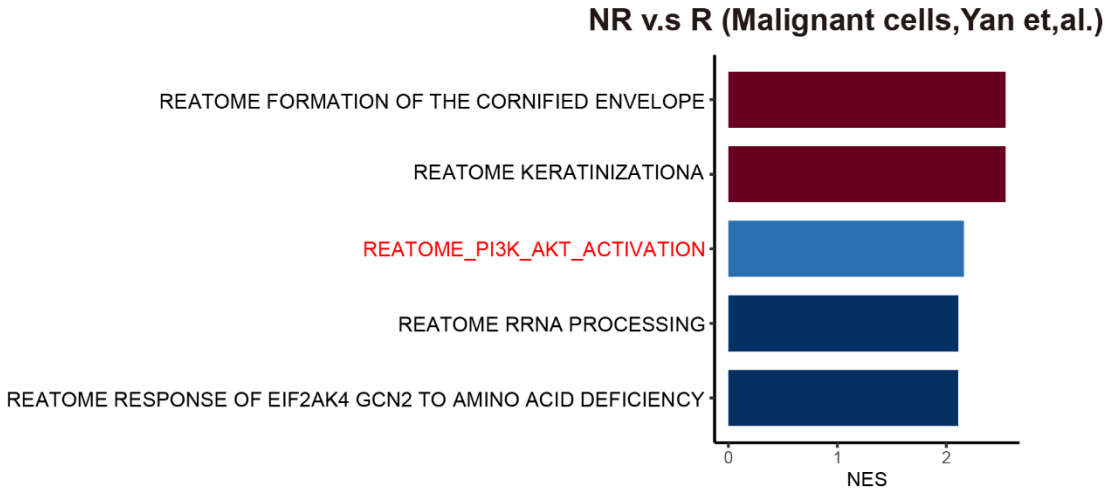

a
A549
Cell viability %
Cisplatin[log, μM]
NC
IC50 = 19.66
siSLC2A1-1
IC50 = 8.368
siSLC2A1-1
IC50 = 8.256
b
H1299
Cell viability %
Cisplatin[log, μM]
NC
IC50 = 26.20
siSLC2A1-1
IC50 = 10.45
siSLC2A1-1
IC50 = 12.77
c
A549
Cell viability %
Cisplatin[log, μM]
NC
IC50 = 18.46
ovSLC2A1
IC50 = 27.83
d
H1299
Cell viability %
Cisplatin[log, μM]
NC
IC50 = 25.97
ovSLC2A1
IC50 = 38.37
e
A549
NC
siSLC2A1-1
siSLC2A1-2
PI
Annexin V-FITC
A549
Apoptosis%
NC
siSLC2A1-1
siSLC2A1-2
f
H1299
NC
siSLC2A1-1
siSLC2A1-2
PI
Annexin V-FITC
H1299
Apoptosis%
NC
siSLC2A1-1
siSLC2A1-2
g
A549
NC
OVSLC2A1
PI
Annexin V-FITC
A549
Apoptosis%
NC
ovSLC2A1
h
H1299
NC
OVSLC2A1
PI
Annexin V-FITC
H1299
Apoptosis%
NC
ovSLC2A1
i
A549
NC
siSLC2A1-1
siSLC2A1-2
A549
Relative migration rate(%)
NC
siSLC2A1-1
siSLC2A1-2
k
A549
NC
ovSLC2A1
A549
Relative migration rate(%)
NC
ovSLC2A1
j
H1299
NC
siSLC2A1-1
siSLC2A1-2
H1299
Relative migration rate(%)
NC
siSLC2A1-1
siSLC2A1-2
l
H1299
NC
ovSLC2A1
H1299
Relative migration rate(%)
NC
ovSLC2A1

Figure 6


a
A549
ovSLC2A1
IC50 = 29.11
ovSLC2A1+AKT inhibition
IC50 = 11.11
Cell viability %
Cisplatin[log，μM]
b
H1299
ovSLC2A1
IC50 = 37.98
ovSLC2A1+AKT inhibition
IC50 = 18.07
Cell viability %
Cisplatin[log，μM]
c
A549
OVSLC2A1
OVSLC2A1+AKT抑制
PI
Annexin V-FITC
A549
Apoptosis%
NC
ovSLC2A1
d
H1299
OVSLC2A1
OVSLC2A1+AKT抑制
PI
Annexin V-FITC
H1299
Apoptosis%
NC
ovSLC2A1
e
A549
ovSLC2A1
ovSLC2A1+AKT抑制
200μm
A549
Relative migration rate(%)
ovSLC2A1
ovSLC2A1+AKT抑制
f
H1299
ovSLC2A1
ovSLC2A1+AKT抑制
200μm
H1299
Relative migration rate(%)
ovSLC2A1
ovSLC2A1+AKT抑制
g
A549
NC
siSLC2A1-2
siSLC2A1-1
PDL1
PDL1 (MFI)
NC
siSLC2A1-1
siSLC2A1-2
h
H1299
NC
siSLC2A1-1
siSLC2A1-2
PDL1
PDL1 (MFI)
NC
siSLC2A1-1
siSLC2A1-2
i
A549
NC
ovSLC2A1
ovSLC2A1+AKT抑制
PDL1
PDL1 (MFI)
NC
ovSLC2A1
ovSLC2A1+AKT抑制
j
H1299
NC
ovSLC2A1
ovSLC2A1+AKT抑制
PDL1
PDL1 (MFI)
NC
ovSLC2A1
ovSLC2A1+AKT抑制

Supplementary Fig.1

a



Supplementary Fig.1 GSEA identifies AKT pathway activation in malignant cells of non-responsive patients. (a) GSEA showing significantly enriched signaling pathways in malignant epithelial cells derived from the NR group compared to the R group from Yan's data. GSEA: Gene Set Enrichment Analysis

Supplementary Files

This is a list of supplementary files associated with this preprint. Click to download.

- wbRawdata.tif